The Astrophysical Journal, 753:117 (16pp), 2012 July 10 doi:10.1088/0004-637X/753/2/117

CHANDRA/ACIS-I STUDY OF THE X-RAY PROPERTIES OF THE NGC 6611 AND M16 STELLAR POPULATIONS

M. G. Guarcello[1], M. Caramazza[2], G. Micela[2], S. Sciortino[2], J. J. Drake[1], and L. Prisinzano[2]
[1] Smithsonian Astrophysical Observatory, MS-67, 60 Garden Street, Cambridge, MA 02138, USA
[2] INAF-Osservatorio Astronomico di Palermo, Piazza del Parlamento 1, 90134 Palermo, Italy
Received 2012 January 27; accepted 2012 May 3; published 2012 June 20

ABSTRACT

Mechanisms regulating the origin of X-rays in young stellar objects and the correlation with their evolutionary stage are under debate. Studies of the X-ray properties in young clusters allow us to understand these mechanisms. One ideal target for this analysis is the Eagle Nebula (M16), with its central cluster NGC 6611. At 1750 pc from the Sun, it harbors 93 OB stars, together with a population of low-mass stars from embedded protostars to disk-less Class III objects, with age $\leqslant$ 3 Myr. We study an archival 78 ks *Chandra*/ACIS-I observation of NGC 6611 and two new 80 ks observations of the outer region of M16, one centered on the Column V and the other on a region of the molecular cloud with ongoing star formation. We detect 1755 point sources with 1183 candidate cluster members (219 disk-bearing and 964 disk-less). We study the global X-ray properties of M16 and compare them with those of the Orion Nebula Cluster. We also compare the level of X-ray emission of Class II and Class III stars and analyze the X-ray spectral properties of OB stars. Our study supports the lower level of X-ray activity for the disk-bearing stars with respect to the disk-less members. The X-ray luminosity function (XLF) of M16 is similar to that of Orion, supporting the universality of the XLF in young clusters. Eighty-five percent of the O stars of NGC 6611 have been detected in X-rays. With only one possible exception, they show soft spectra with no hard components, indicating that mechanisms for the production of hard X-ray emission in O stars are not operating in NGC 6611.

Key words: open clusters and associations: individual (NGC 6611 and M16) – stars: coronae – stars: massive – stars: pre-main sequence – X-rays: stars

Online-only material: color figures

1. INTRODUCTION

Since the discovery of the intense X-ray emission from young pre-main-sequence (PMS) stars (Feigelson & Decampli 1981; Montmerle et al. 1983), X-ray observations of active star-forming regions and young galactic clusters have become an efficient method of studying the star formation process and the properties of young stars. In fact, the level of X-ray emission in PMS stars, which is higher than that of field main-sequence stars, provides a very efficient means of selecting stars associated with star-forming regions and young clusters. In the last decade, a large number of young clusters have been observed with X-ray telescopes, such as the *Chandra X-ray Telescope* (Weisskopf et al. 2002) and *XMM-Newton* (Jansen et al. 2001), in order to select their young members and study their X-ray activity. To the present day, the longest X-ray observations of star-forming regions have been the 839 ks Chandra Orion Ultradeep Project (COUP; Getman et al. 2005), the 1.08 Ms Chandra Cygnus OB2 Legacy Survey (Drake et al. 2009), and the 1.6 Ms Chandra Carina Complex Project (Townsley et al. 2011a).

While we have a reasonably detailed comprehension of the coronal activity and accretion phenomenon in low-mass PMS stars, and of the mechanisms for X-ray emission in massive stars, several key topics are still not completely understood. These topics include how the presence of a circumstellar disk affects X-ray activity (Flaccomio et al. 2003), the nature of the huge spread in X-ray activity observed in almost all the young clusters (Feigelson et al. 2002), and the importance of the proposed mechanisms for hard X-ray emission in massive stars (Babel & Montmerle 1997).

In this paper, we address some of these topics by studying the global X-ray properties of the young stars associated with the Eagle Nebula (M16) and its central cluster NGC 6611. Situated in the Sagittarius arm and lying in the southern sky, this cluster is 1750 pc away from the Sun. It suffers only a low average extinction in the central cavity of the molecular cloud cleared by the cluster itself ($A_V \sim 2.6^m$; Guarcello et al. 2007), but becomes more absorbed in the surrounding area where the cloud is still dense (Guarcello et al. 2010b). The central cluster hosts 93 OB stars (Hillenbrand et al. 1993), including one of the rare candidate O4 stars observed in our galaxy (W205, with a mass of 75–80 $M_\odot$; Evans et al. 2005); the massive binary system W175, composed of an O5V star (Evans et al. 2005) and a late-O (likely O8.5) star (Martayan et al. 2008); some Herbig Ae/Be stars; and the two magnetic stars W080 (B1V) and W601 (B1.5) (Martayan et al. 2008; Alecian et al. 2008).

The region is also rich in PMS stars with low and intermediate masses. In our previous studies of this region (Guarcello et al. 2007, 2009, 2010a, 2010b), we detected a total of 1937 candidate PMS stars associated with M16. The disk-less stars have been selected from their intense X-ray emission and the disk-bearing stars from their excesses in infrared bands. The X-ray-selected young stars of NGC 6611 have a median age of $\sim$1 Myr (Guarcello et al. 2007), but in the whole cloud a star formation sequence has been proposed (Guarcello et al. 2010b) with the oldest star formation events to the southeast ($\sim$3 Myr) and the youngest in the northwest ($<$1 Myr). Together with these large populations of Class II and Class III objects, a significant number of embedded Class 0/I sources (Indebetouw et al. 2007), water masers (Healy et al. 2004), and candidate Herbig–Haro objects (Meaburn & Walsh 1986) have been identified in sites of M16 with ongoing star formation activity, such as the structures called "the Pillars of Creation" and "Column V" (Hester et al. 1996; McCaughrean & Andersen 2002; Sugitani et al. 2007), the

Bright Rimmed Cloud (BRC) SFO30 northward of the cluster, and a young cluster in the northeast largely embedded in the molecular cloud (Indebetouw et al. 2007; Guarcello et al. 2009).

The Eagle Nebula hosts a large variety of young X-ray-emitting sources whose X-ray properties will be studied in detail in this paper. Our scope is to characterize the global X-ray properties of the cluster, to study how X-ray activity of cluster members is affected by the presence of the disks, and finally to take advantage of the large massive-star population of NGC 6611 to study X-ray emission in OB stars. The paper is organized as follows: In Section 2 we review the data analysis, source detection, the identification of the stellar counterparts of the detected X-ray sources, and the spectral analysis. The distributions of plasma temperature and hydrogen column density of the M16 stars are analyzed in Section 3. The X-ray luminosity function (XLF) of the whole population, as a function of the stellar mass and of evolutionary status, is studied in Section 4. In Section 5, we study the X-ray emission of massive stars; and in Section 6, we review the X-ray properties of the stellar population of selected regions of the Eagle Nebula. In the Appendix, we present the X-ray catalog of detected sources.

2. DATA ANALYSIS AND CATALOG

2.1. Source Identification and Photon Extraction

Figure 1 shows the image of the Eagle Nebula in the *I* band obtained with the Wield Field Imager mounted on the 2.2 m telescope at ESO (Guarcello et al. 2007). The contours mark the dust emission detected at 8.0 μm with *Spitzer*/IRAC (Indebetouw et al. 2007; Guarcello et al. 2009), marking the Pillars of Creation, the Column V, and the SFO30 cloud (the outer contours delimit the size of the used IRAC image). The rotated squares represent the fields observed with *Chandra*/ACIS-I. The archival observation of 78 ks (Linsky et al. 2007) is centered on NGC 6611 (the *c-field*), and it includes the Pillars of Creation and the SFO30 cloud. The two new observations of 80 ks (P.I: Guarcello) are centered on Column V (the *e-field*), and on a group of Class I and embedded Class II stars (the *ne-field*) that is younger than 1 Myr.

X-ray image reduction and source detection in all the fields are described in Guarcello et al. (2010b), where detected X-ray sources (1158, 363, and 315 in the *c*-, *e*-, and *ne-fields*, respectively) with their optical–NIR counterparts have been used to classify young stellar objects (YSOs) in this region. Briefly, for each observation a *Level 2* event file has been obtained using the CIAO 4.0[3] tool *acis-process-events*, retaining only the events incompatible with cosmic rays and removing the 0.″5 event position randomization added by the standard Chandra data processing pipeline. Source detection has been performed with PWDetect[4] (Damiani et al. 1997) adopting a threshold corresponding to 10 spurious detections. The total number of detected X-ray sources is 1755 (81 sources are in the overlapping region between the *c-field* and the *e-field*). As described in Guarcello et al. (2010b), the mass limit of the X-ray sources with optical counterparts (for which it was possible to estimate the mass) is equal to 0.2 $M_{\odot}$. Figure 1 shows the photon extraction regions of each detected source. The clustering of sources in NGC 6611 is evident, but this image clearly shows that the outer parts of the nebula are also well populated by young stars.

[3] http://cxc/harvard.edu/ciao
[4] http://www.astropa.unipa.it/progetti_ricerca/PWDetect

Photon extraction has been made using the IDL software ACIS Extract[5] (AE; Broos et al. 2010), which uses TARA,[6] CIAO, FTOOLS,[7] and MARX[8] packages. AE calculates the point-spread function (PSF) for each source, using it to define a photon extraction region as the region encompassing 90% of the PSF evaluated at 1.49 keV. Background events have been extracted for each source in circular annuli centered on the sources, applying a mask for source counts defined in two iterations (first a circular area covering 99% of the local PSF and then with a more accurate mask region). The extraction regions of crowded sources are reduced to avoid overlapping each other, down to 40% of the local PSF in the most crowded regions. In this first phase, AE uses the source positions provided by the source detection algorithm (PWDetect in our case). Once both the PSF and the background for each source are evaluated, AE computes new source positions by correlating the source images with the local PSF model. The user has the possibility to use these new positions or retain the set of positions provided by the source detection algorithm. As suggested by the AE manual, we updated the positions of the sources observed with an off-axis larger than 5′ (further coordinate corrections of $\Delta_{\alpha} = -0.''18$ and $\Delta_{\sigma} = -0.''05$ have been applied to cross-correlate the X-ray catalog with the optical–infrared catalog; see Section 2.2). AE then repeats the computation of the PSF and the background and the photon extraction using the new positions. For each source, AE provides information such as the net observed counts, the light curves, and a probability that the observed light curve is constant based on a Kormogorov–Smirnov test; the most relevant is summarized in the electronic catalog described in the Appendix.

2.2. Stellar Counterparts of the X-Ray Sources

Detected X-ray sources are classified in Guarcello et al. (2010b) according to the properties of their optical/infrared counterparts. Among the 834 sources with disks, selected by their NIR excesses with respect to the expected photospheric emission, 219 have an X-ray counterpart and are classified as "disk-bearing members." We classified as "disk-less members" 964 X-ray sources that are younger than 10 Myr and have an extinction higher than 2.6^{m}, according to their position in the optical color–magnitude diagram. A total of 76 sources are older than 10 Myr and/or have extinction smaller than 2.6^{m}. These sources are most likely foreground main-sequence stars detected in X-rays, which are then classified as "foreground sources." A total of 504 X-ray sources are not identified with a known stellar counterpart. In Guarcello et al. (2010b), we compared our count-rate limit (6.25×10^{-5} counts s^{-1}), properly converted into a limit flux in the 0.5–10 keV energy band, with the $\log N$ vs. $\log S$ distribution of extragalactic sources in the ELAIS field shown in Puccetti et al. (2006), estimating an upper limit of the observed extragalactic X-ray sources equal to 193.5. We then expect that about 300 X-ray sources without optical–infrared counterparts can be very embedded sources associated with M16 (a significant fraction of them lie in the regions with high extinction, such as the *ne-field*) or background sources lying in our Galaxy. Since we cannot discern among these hypotheses, we simply classified them as "background sources" and have not considered them in our study of the global X-ray properties of the M16 population.

[5] http://www2.astro.psu.edu/xray/docs/TARA/ae_users_guide.html
[6] http://www2.astro.psu.edu/xray/docs/TARA/code.
[7] http://heasarc.gsfc.nasa.gov/docs/software/ftools
[8] http://space.mit.edu/CXC/MARX/

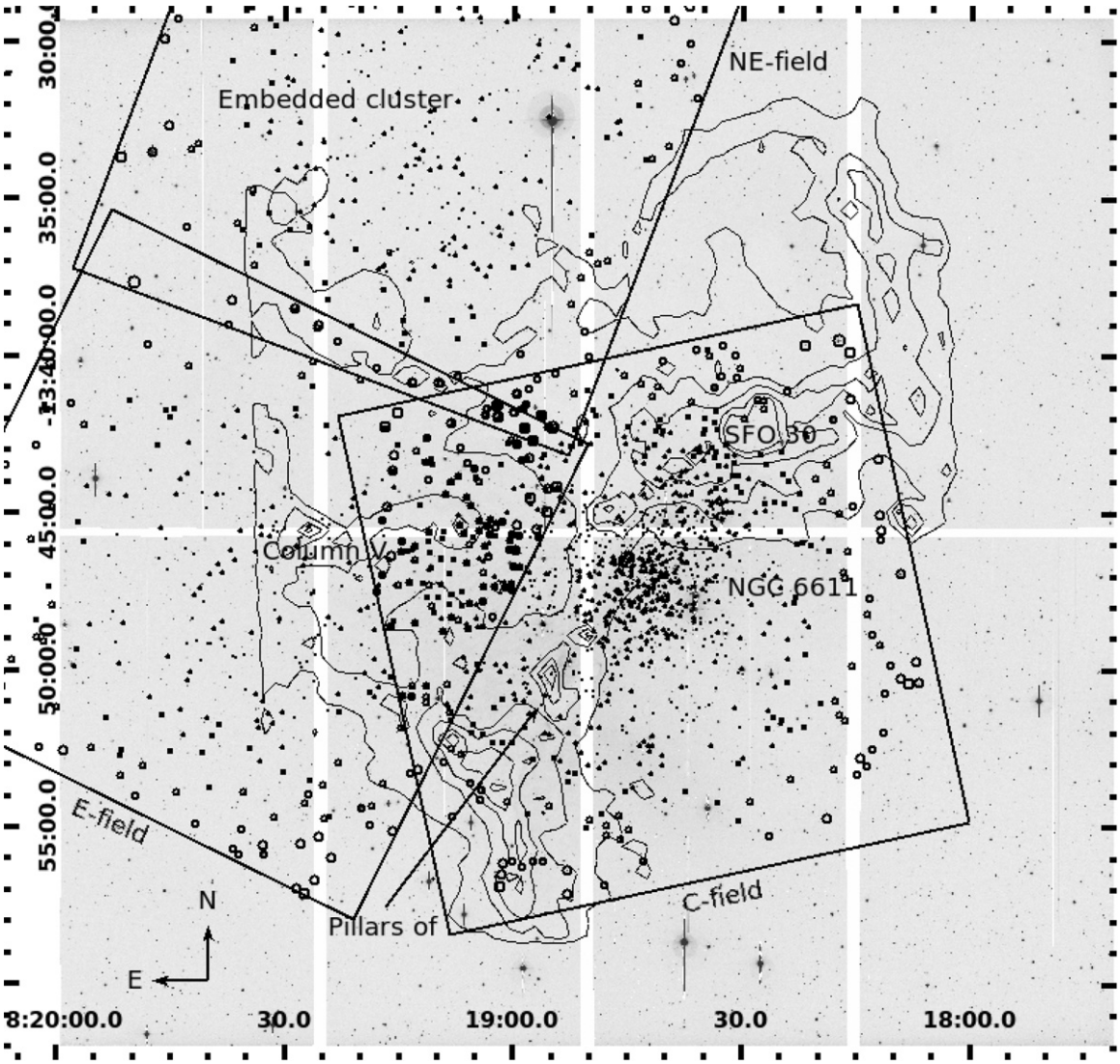

Figure 1. Image in *I* band of M16, with the contours encompassing the emission at 8.0 μm obtained from *Spitzer*/IRAC. The rotated squares are the *Chandra*/ACIS-I fields of the observations analyzed in this work. The black circles mark the positions of detected X-ray sources. The radius of each circle is proportional to the PSF area at the source's position. The positions of Pillars of Creation, Column V, the SFO30 cloud, the northeast embedded cluster, and NGC 6611 are also shown.

Figure 2 shows the spatial distributions of these four classes of X-ray sources. The disk-bearing stars are clearly clumped in NGC 6611 toward Column V and in the embedded northeast cluster. The disk-less members are more numerous and are distributed across the whole cloud. Also, the background sources are sparse in the field, but the high concentration of them in the regions with the highest extinction and embedded ongoing star formation activity (the *ne-field*, eastward the Column V, and in the tip of the Pillars of Creations and Column V) is consistent with the idea that most of these sources are very embedded young stars associated with M16.

2.3. Spectral Analysis: Spectral Fitting

The determination of the absorption corrected X-ray luminosity (L_X), as well as the plasma temperature (kT) and hydrogen column density (N_H), requires the analysis of the X-ray spectra. AE provides both the source and background spectra, the redistribution matrix files, and the ancillary response files. We fit the observed spectra with thermal plasma (with both one and two temperatures) and power-law models. We use the APEC ionization-equilibrium thermal plasma code (Smith et al. 2001), assuming the sub-solar elemental abundances of Maggio et al. (2007). The absorption was treated using the WABS model (Morrison & McCammon 1983). The one-temperature (1T) thermal model was applied to all the sources with more than 25 counts, while the two-temperature (2T) thermal model was applied to each source with more than 80 counts. The power-law model has been applied to those sources with hard spectra for which the best-fit thermal model predicts a plasma temperature $kT > 5$ keV. In order to avoid false convergences due to local minima in the χ^2 space, we applied different sets of initial values to each model. When more than one model has been used for a given source, we chose the best model by the χ^2 probability and visual inspection of the spectrum.

In the *c-field* we were able to obtain a good spectral fit for 441 sources, 114 in the *e-field* and 60 in the *ne-field* (out of a total of 1158, 363 and 315 sources, respectively), for a total of 575 sources with a good spectral fit (40 sources in the overlapping regions). For 33 sources the best-fit model is a two-temperature thermal plasma model. For a total of 20 sources the best-fit model is a power-law spectrum: 15 of them are classified as "background sources," and the remaining 5 are classified as "disk-less members."

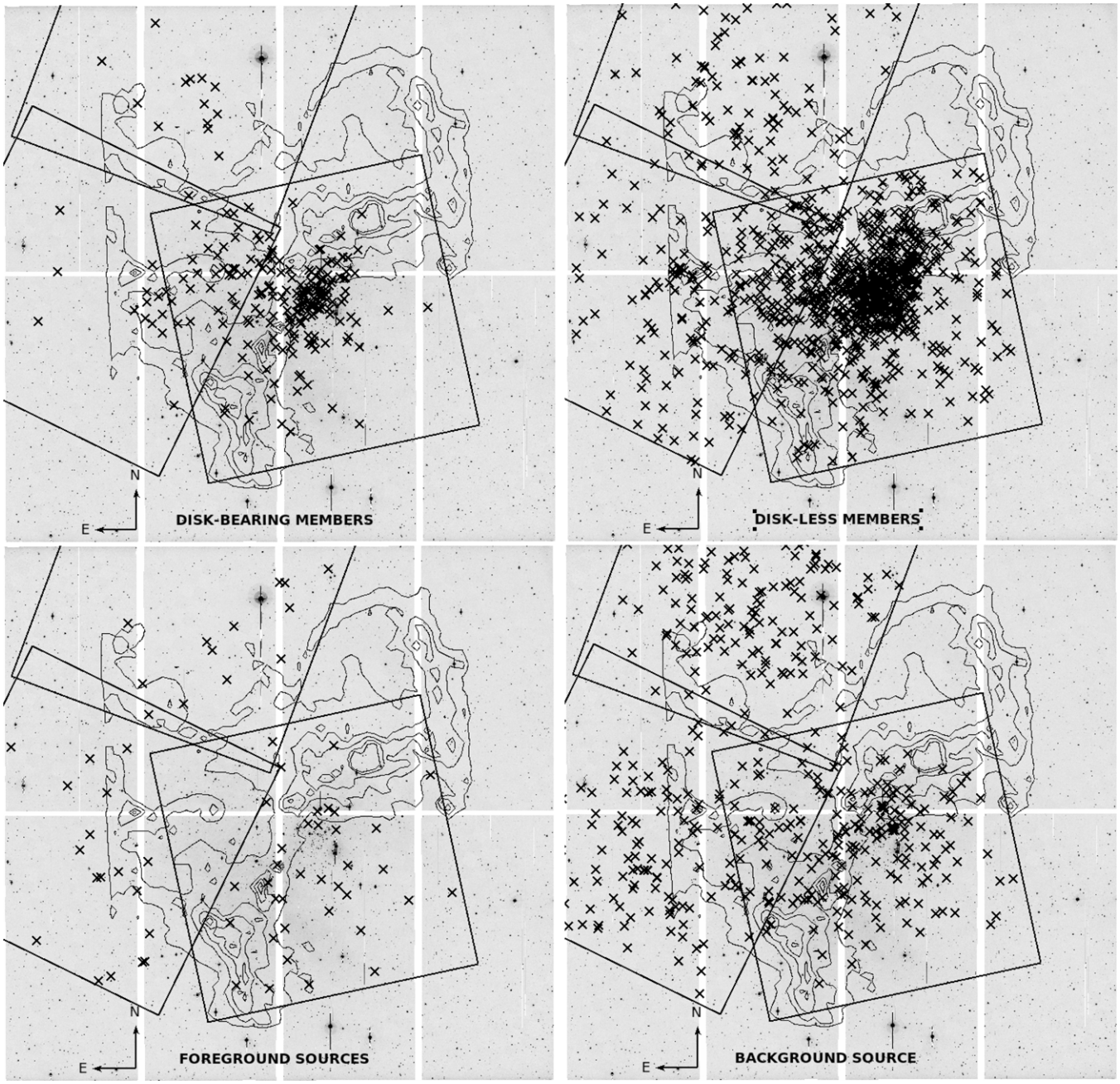

Figure 2. Spatial distribution of the four classes of X-ray sources discussed in Section 2.2 (disk-bearing and disk-less members, foreground and background sources), overplotted with the contours from the [8.0] and the ACIS field used in Figure 1.

2.4. Spectral Analysis: Energy Quantiles

Spectral analysis cannot be performed for faint sources. For them, an estimate of the X-ray luminosity can be provided by the analysis of the photon energy quantiles (Hong et al. 2004). This method is similar to the analysis of the X-ray hardness ratio adopted in several works, but it does not suffer the drawback of the choice of the energy bands used to define the "X-ray colors." Adopting the definition by Hong et al. (2004), if $x\%$ is the percentage of the total counts with energy below the value $E_{x\%}$, the quantile Q_x is defined as

$$Q_x = \frac{E_{x\%} - E_{\rm lo}}{E_{\rm up} - E_{\rm lo}}, \quad (1)$$

where $E_{\rm lo}$ and $E_{\rm up}$ are the lower and upper limits of the energy range, respectively, 0.5 keV and 8.0 keV in our case. We used the median energy (i.e., the 50% quartile) and the 25% and 75% quartiles, which are combined in the following independent variables: $\log(Q_{50}/(1 - Q_{50}))$ and $3 \times (Q_{25}/Q_{75})$. In order to estimate the values of $N_{\rm H}$ and kT for each source, the observed quantile variables have been compared (by interpolation) with a theoretical grid of thermal models with sub-solar abundances and a grid of power-law models with spectral indices typical of active galactic nuclei (AGNs; Brandt et al. 2001).

Figure 3 shows the thermal and power-law grids and the quantiles of the X-ray sources (only the sources with a significance larger than 2 are shown; see the Appendix) for the four groups of sources defined in Section 2.2. The thermal models have a plasma temperature ranging from 0.3 keV to 10 keV and

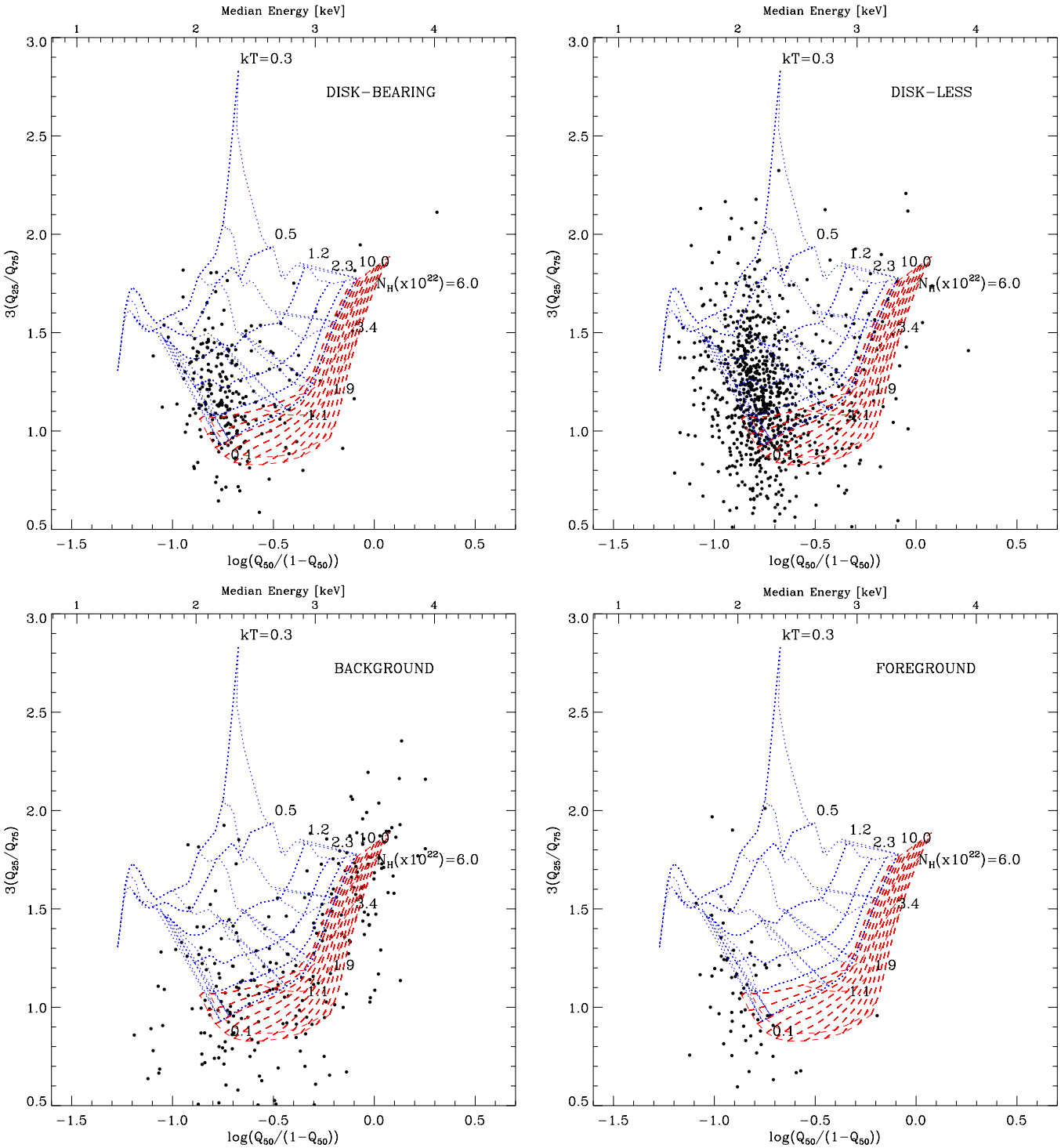

Figure 3. Quantiles of the four classes of X-ray sources, overplotted with the grids derived from thermal one-temperature spectra (blue lines) and power-law spectra (red lines). Some of the values of $N_{\rm H}$ and kT for the thermal models are shown. The power-law models have indices ranging from 0 to 2.0 and the same $N_{\rm H}$ of the thermal models.

(A color version of this figure is available in the online journal.)

hydrogen column density from $0.01 \times 10^{22}\,{\rm cm}^{-2}$ to $6 \times 10^{22}\,{\rm cm}^{-2}$; the power laws have the same hydrogen column density range and a photon index ranging from 0.1 to 2.0. The actual grids used for the interpolations are finer than those shown in Figure 3.

The disk-bearing and disk-less sources (upper panels) are mostly concentrated in the region with $1.2\,keV \leqslant kT \leqslant 4\,{\rm keV}$ and from $0.1 \times 10^{22}\,{\rm cm}^{-2} \leqslant N_{\rm H} \leqslant 1.1 \times 10^{22}\,{\rm cm}^{-2}$, corresponding to a wide range of visual extinction. Both the background and foreground sources are mostly outside the thermal grid. The distribution of the latter suggests values of $N_{\rm H}$ smaller than those used for the grid. The former mostly show harder spectra and are, in most cases, compatible with power-law models. However, from the grid it is not possible to

discriminate the real extragalactic sources from the embedded cluster members, given the degeneracy between very hard thermal spectra and power laws.

A close inspection of Figure 3 shows the presence of eight background sources in the area of the soft thermal spectra corresponding with $kT < 0.5$ keV. Even if they are not very bright (the median net counts of this sample is 19), the probability associated with the hypothesis that they are spurious detections is negligible (see the *PBS* parameter, explained in the Appendix). Five of these sources lie in the *c-field* and have a median photon energy between 1.3 keV and 1.8 keV. It is not obvious what these sources are. One intriguing possibility is that some of them are compact objects associated with M16 and are remnants of the explosion of a massive star. The possibility that M16 hosted a supernova explosion in the past has been suggested by Flagey et al. (2011) to explain the hot dust (∼70 K) they observed in the cloud. However, NGC 6611 is not old enough to firmly claim that the most massive members already exploded as supernovae, and the median photons energy of these eight sources is higher than that of the candidate neutron stars recently identified in the Carina complex by Townsley et al. (2011b).

In total, 846 sources lie inside the thermal grid. For these sources the individual values of $N_{\rm H}$ and kT have been calculated by interpolating their quantile variables in the thermal grid and then their X-ray luminosity, L_X, using the distance adopted for the cluster (1750 pc; Guarcello et al. 2007) and correcting for the individual absorption. To estimate the uncertainties in the X-ray stellar parameters from the grid, we calculated the errors in their photons energy quantiles, following the procedure of Hong et al. (2004), and propagated to the independent quantile quantities. Then, we repeated the interpolation with the grid four times, each time with a different combination of sum and subtraction of the errors to the quantile quantities. In this way, for each star and for each parameter we had four slightly different values. For each nominal value (i.e., those derived from the grid without adding or subtracting the errors) of the three quantities, the upper error has been defined as the difference between the maximum of these four measures and the nominal value, the lower error as the difference with the minimum value. The median errors for the three parameters are $\sigma_{N_{\rm H}} = 0.7\,{\rm cm}^{-2}$, $\sigma_{kT} = 0.4$ keV, and $\sigma_{\log(L_X)} = 0.3\,{\rm erg\,s}^{-1}$.

A total of 312 sources lie inside the power-law grid, and, as shown in Figure 3, 82% of them are background sources (with a wide range of hydrogen column density) and disk-less stars. There are 346 sources lying outside both grids. Most of them have $3Q_{25}/Q_{75}$ smaller than those of the grid models. Hong et al. (2004) suggested that low significance sources can fall in the area of the diagram with $3Q_{25}/Q_{75} < 0.8$. In fact, the sources in this region of the diagram have a median of 12 counts, indicating they mostly fall in this region because of low counts.

2.5. Upper Limits

The main aim of this paper includes the comparison between the X-ray properties of disk-less and disk-bearing stars, the study of the global X-ray properties of the M16 population, and their comparison with those of the Orion members. A reliable comparison requires knowledge of the upper limit of X-ray luminosity for the undetected members. The problem of the incompleteness of the sample of Class III objects of M16 will be discussed later, since we do not know the X-ray-undetected Class III stars. This is not the case for the disk-bearing members, since we have detected in X-rays 219 sources with infrared excesses out of a total of 834 previously identified sources. The upper limit of the photon count rate at the positions of the undetected disk-bearing stars is calculated with PWDetect, adopting the same threshold significance used for source detection. We have converted these upper limit count rates to X-ray luminosity using as a conversion factor the median of the ratio between the X-ray luminosities and photon count rates for the detected members.

3. PLASMA TEMPERATURE AND HYDROGEN COLUMN DENSITY OF M16 MEMBERS

In the following sections, we will address several facets of the X-ray properties of M16 members, starting from the distributions of plasma temperatures and absorption. As explained in the previous sections, values of $N_{\rm H}$ and plasma temperature are associated with the X-ray source from the spectral fitting or quantile analysis. When a good fit with a thermal model is available, these values and their uncertainties are adopted from the best-fit model. In the other cases, they are taken from the interpolation in the thermal grid (as shown in Figure 3) for the sources that lie inside the grid. For those sources without a good spectral fit with a thermal model (1T or 2T) and whose position in the diagrams in Figure 3 is outside the thermal grid, no values of $N_{\rm H}$ and plasma temperature are provided.

Figure 4 shows the distributions of $N_{\rm H}$, kT, and median photon energy of the X-ray sources in M16 (both disk-less and disk-bearing sources). The $N_{\rm H}$ distribution covers a large range of values with a median value corresponding to $A_V = 3.6^m$, which is larger than the average extinction estimated by Guarcello et al. (2007) from the analysis of the optical diagrams ($A_V = 2.7^m$). We will show in Section 6 that the discrepancy between these two estimates is reduced by considering the stars in the central cavity cleared by NGC 6611. Part of the large spread of the $N_{\rm H}$ distribution is purely statistical, but since about 55% of the sources with lowest $N_{\rm H}$ are clustered in the cavity cleared by NGC 6611 or southward (where the extinction is lower; see Guarcello et al. 2010b), while a similar fraction of the sources with highest $N_{\rm H}$ mostly lie in the trunks, in the SFO30 cloud, and in the northeast, part of the spread in the $N_{\rm H}$ distribution is due to the strong differential reddening across the nebula.

The median values of both kT and median photon energy are similar to those observed in other star-forming regions (for instance in Orion, Feigelson et al. 2002; in NGC 1893, Caramazza et al. 2012). The two populations of sources with $kT < 1.14$ keV and $kT > 4.09$ keV (which are the quantiles at 80% and 20% of the kT distribution), have different fractions of variable sources, suggesting that part of the spread observed in the kT distribution can be due to X-ray variability, with some sources observed during periods of quiescent emission and others during flares. In fact, by adopting a threshold for variability of $P_{\rm K-S} < 0.005$ (see the Appendix), 42% of the sources in the high-temperature tail of the kT distribution can be variable, while among those with $kT < 1.14$ keV only 14% can be variable. This suggests a larger contribution from flares in the X-ray emission of the sources with highest plasma temperature. Besides, the presence of sources with high plasma temperature ($kT > 4.09$) among those with a constant light curve and low luminosity supports the hypothesis that "quiescent" X-ray emission from magnetically active stars can arise from the merging of coronal microflares (Drake et al. 2000; Caramazza et al. 2007).

Figure 5 shows the distributions of $N_{\rm H}$, plasma temperature, and median photon energy separately for sources in the *c-field* (left panel), *e-field* (central panel), and *ne-field* (right panel).

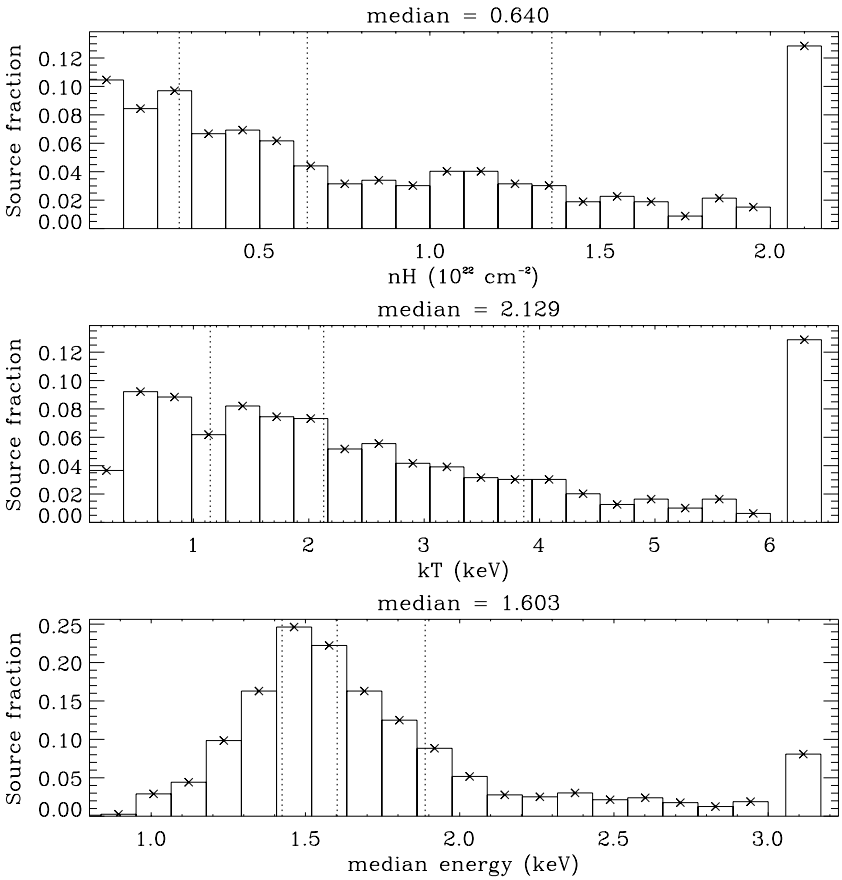

Figure 4. Distributions of the $N_{\rm H}$, kT, and median photon energy for the X-ray sources in M16. The dotted vertical lines mark the 25%, 50%, and 75% quartiles of each distribution.

The distributions for the populations of the *c-field* and *e-field* are similar, reflecting the similar age and extinction in these two fields as found by Guarcello et al. (2010b). The largest differences arise in the *ne-field*, where the median hydrogen column density is $N_{\rm H} = 1.4 \times 10^{22}$ cm^{-2}, corresponding to $A_V = 7.98^m$, which is higher than the extinction and median $N_{\rm H}$ found in the other two fields (3.2^m). This mostly explains the lack of sources with soft spectra in the *ne-field* compared with the other two fields, and the higher kT median value (2.86 keV versus 2.01 keV and 2.12 keV).

4. X-RAY LUMINOSITY OF M16 MEMBERS

4.1. The X-Ray Luminosity Function

X-ray luminosities and their uncertainties have been obtained from the spectral or quantile analysis with the same criteria adopted for plasma temperature and hydrogen column density (Section 3). In addition, for the sources without a good spectral fit and that are outside the thermal grid in the diagrams in Figure 3, they have been inferred directly from the count rates, using as a conversion factor the median $L_X/(count\_rate)$ ratio found for the other sources (which ranges from 7×10^{33} to 1×10^{34} in the three fields).

The total luminosity of M16 is equal to $\log(L_X) = 34.90$ erg s^{-1}, with an individual source median value of $\log(L_X) = 30.4^{+0.1}_{-0.6}$ erg s^{-1}. In this estimate, we excluded a candidate disk-less member with very high luminosity $\log(L_X) = 34.1^{+0.1}_{-0.5}$ erg s^{-1}. This luminosity, in fact, is apparently too high to be correct, since it is two orders of magnitude higher than the L_X of the second most luminous star in our sample. Its spectrum has been fitted with a two-temperature thermal model, with a soft primary component ($kT_1 = 0.11 \pm 0.01$ keV) and a harder secondary component with $kT_2 = 1.7 \pm 0.6$ keV, but the emission measure of the hard component is 10^5 times fainter than that of the soft component. One possibility is that this is a foreground source with an overestimated distance or a background high-mass X-ray binary, but both the $N_{\rm H}$ value (equal to 4.45×10^{22} cm^{-2}) and its position in the optical color–magnitude diagrams suggest a young and embedded star lying in the BRC-SFO30.

Figure 6 compares the X-ray luminosity calculated from the quantile analysis with that from the spectral fits, for the sources in our sample with a good significance and a spectral fit with good χ^2. The estimate of L_X from the quantile analysis agrees with that from the spectral analysis for most of the stars in Figure 6, with the exception of few outliers. These outliers mostly lie in the low kT–high $N_{\rm H}$ region of the grid, where the low sensitivity of the ACIS detector to the soft part of the spectrum results in large uncertainty in estimates of $N_{\rm H}$ and kT.

One of the aims of this paper is to verify whether the XLF of M16 confirms the universality of the XLFs in clusters younger than a few Myrs, as a consequence of the very slow decline of the X-ray luminosity for PMS stars younger than 10 Myr (Preibisch & Feigelson 2005). Several authors compared the XLFs of young clusters with that observed in the Orion Nebula Cluster (ONC) in the COUP survey, which is the most complete X-ray observation of a young cluster, complete down to 0.1 $M_\odot$ (Getman et al. 2005). A good agreement was found in IC348 and NGC 1333 (2–3 Myr; Feigelson et al. 2005; Winston et al. 2010), M17 (∼1 Myr; Broos et al. 2007), NGC 6357 (∼2 Myr;

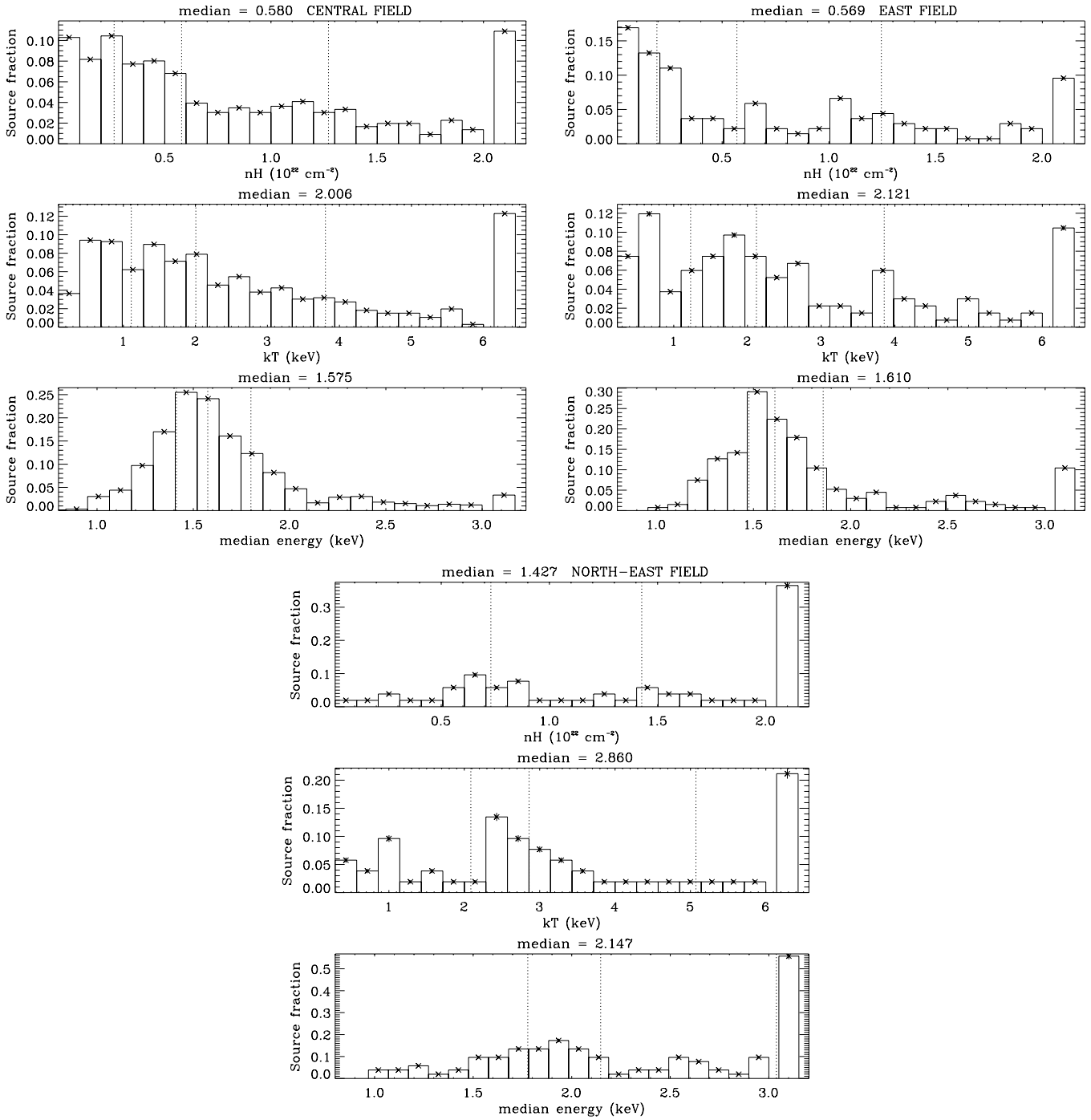

Figure 5. Distributions of the $N_{\rm H}$, kT, and median energy of the X-ray sources in M16 falling in the three observed fields. The dotted vertical lines mark the 25%, 50%, and 75% quartiles of each distribution.

Wang et al. 2007), NGC 2244 (2–3 Myr; Wang et al. 2008), and Cyg OB2 (3–5 Myr; Wright et al. 2010). In this paper we adopt the same approach, comparing the XLF of M16, where the X-ray-emitting population has an age ranging from <1–3 Myr (Guarcello et al. 2007), with that of the ONC.

Figure 7 shows the XLF we obtained for M16, together with that of the COUP sources in Orion. The latter is almost constant for $\log(L_X) < 30\,{\rm erg\,s^{-1}}$, while the M16 XLF drops below this limit, which turns out to be the completeness limit of our observations. For luminosities higher than the completeness limit, the XLF of M16 can be fitted with a power law with index $\Gamma = -0.85 \pm 0.09$, which is consistent with that of the Orion XLF ($\Gamma = -0.93 \pm 0.08$; Feigelson et al. 2005) in the same luminosity range. In this calculation, we have not considered the OB stars detected in X-rays, since the Orion OB population is significantly different from that of M16.

The comparison between the XLFs of Orion and M16 can help us to estimate the level of incompleteness of our sample of members down to the subsolar limit. To match the Orion XLF with the M16 XLF, we have to scale the former by 1.7. The total Orion population with $M > 0.1\,M_{\odot}$ counts 1600 members (Getman et al. 2005). The match between the two XLFs suggests a total M16 population of 2700 members, larger than the number of members we identified in our previous work (1907 in total,

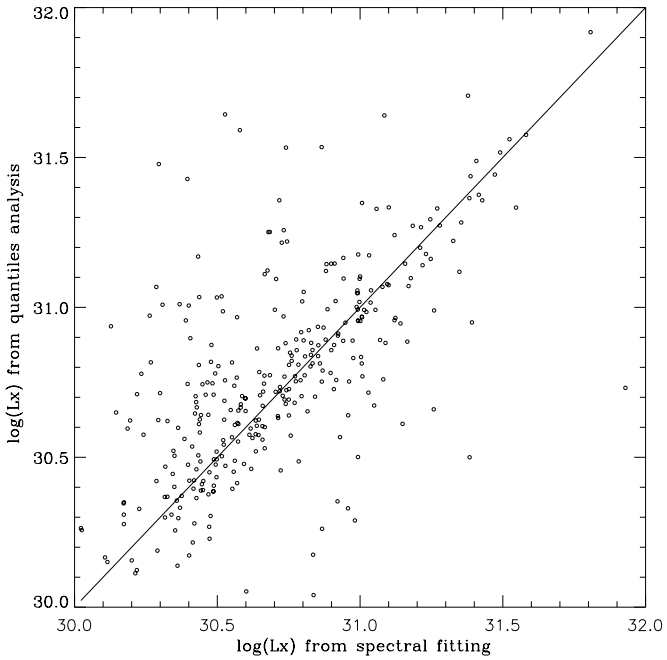

Figure 6. Values of the X-ray luminosity (in erg s^{-1}) calculated from the quantile analysis vs. the values obtained from spectral fitting for the X-ray sources in our sample.

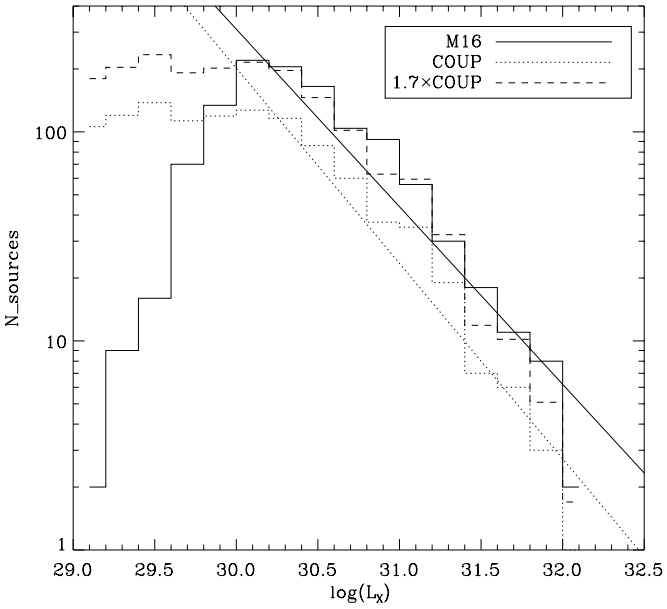

Figure 7. X-ray luminosity functions for M16 and Orion members. The dashed histogram is the Orion XLF scaled up to the M16 XLF. The continuous and dotted lines show the slopes of the linear fits of the XLFs for $\log(L_X) > 30$ erg s^{-1}.

incomplete for a low-mass regime). This is a rough estimate of the still unidentified M16 population, since it depends on several properties of M16 and ONC, such as the physical extent and absorption characteristics in the respective sky areas that are not compared properly here.

4.2. X-Ray Luminosity and Stellar Mass

In young PMS stars, L_X is generally observed to increase with the stellar mass, due to the fact that the dynamo mechanism in PMS stars is in the saturated regime, which means that it is independent of the rotational velocity and it depends only

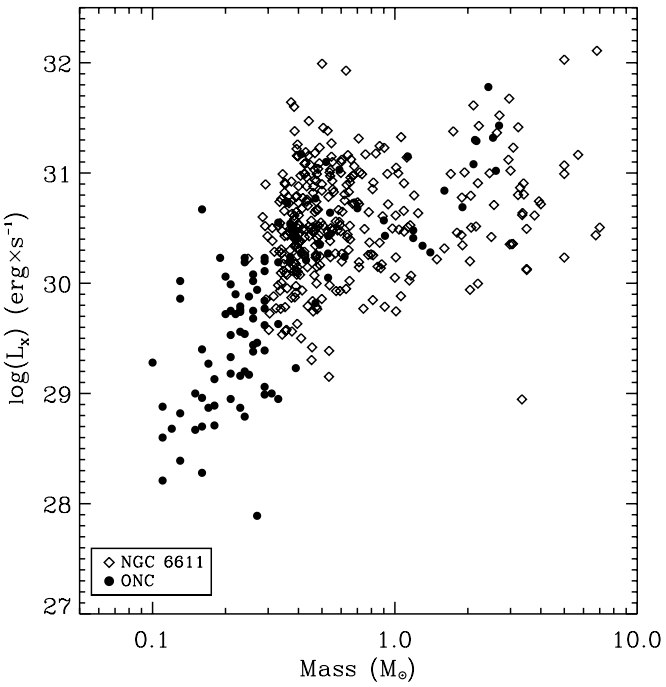

Figure 8. $\log(L_X)$ vs. mass for the detected Class III members in M16 (diamonds) and Orion (dots).

on the stellar mass and bolometric luminosity (Preibisch & Feigelson 2005). To study the L_X versus mass relation in M16, we estimated the masses of M16 members with optical and X-ray detections, first obtaining their intrinsic optical photometry using the extinction map of M16 obtained in Guarcello et al. (2010b), then finding both stellar mass and age by interpolating the dereddened V and $V-I$ with the colors expected from the grid of isochrones of Siess et al. (2000). In this study, we focused only on the Class III stars, since the mass estimate from the optical photometry in Class II objects can be affected by the presence of the disk (Guarcello et al. 2010a).

Figure 8 shows the L_X versus mass scatter plot for Class III stars in M16 and Orion (Getman et al. 2005). In each mass bin, there is a large spread of L_X of about 1.5–2 orders of magnitude. This spread is mostly statistical, but binarity can also play a role (Feigelson et al. 2002). The distribution of the low-mass stars in M16 (i.e., with $M \leqslant 0.8\,M_\odot$) follows the L_X versus mass relation valid in Orion. In fact, a linear fit in this range of mass gives

$$\log(L_X) = (30.9 \pm 0.1) + (1.1 \pm 0.3) \cdot \log(M/M_\odot) \qquad (2)$$

with a slope consistent with that found in Orion (Preibisch & Feigelson 2005). Given the consistency of the two XLFs and assuming the universality of the initial mass function (IMF), the fact that the *low-mass* population of M16 and ONC follows the same L_X versus mass relation is not surprising.

In Figure 8, the distribution of stars more massive than $0.8\,M_\odot$ is totally different, being flatter (with a slope of 0.4 ± 0.2) than that in the low-mass regime. Similar behavior has been observed in other young clusters. Our data do not allow us to understand the nature of the flattening of the L_X versus mass distribution observed at about $1\,M_\odot$. The most likely explanation is that it is due to changes in stellar interior. Feigelson et al. (2003), following the models of Palla & Stahler (1993), have shown as in the mass range between $2.4 < M/M_\odot < 3.9$, very young PMS stars have already developed a radiative core, surrounded by a

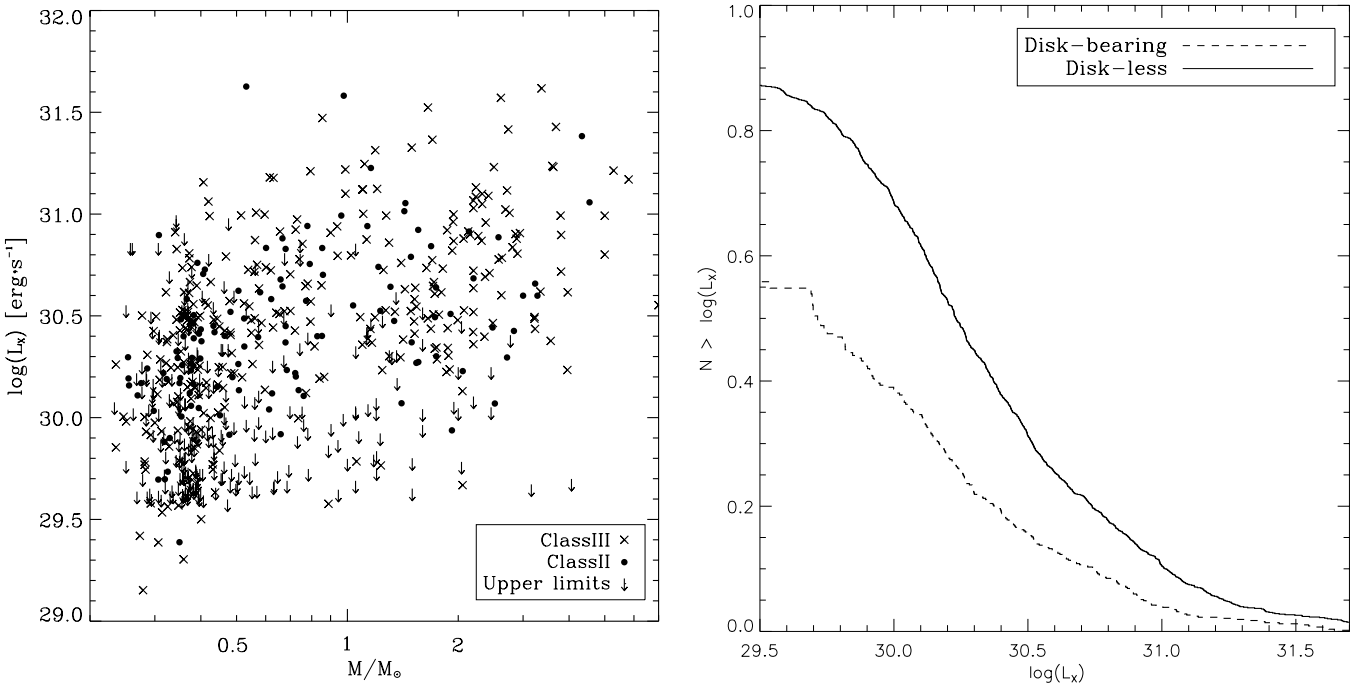

Figure 9. Left panel: $\log(L_X)$ vs. $M/M_\odot$ for the Class III (crosses), Class II (filled dots), and upper limits (arrows) in M16. Right panel: X-ray luminosity function for completed Class III and Class II sources with mass in the $0.2 \leqslant M/M_\odot \leqslant 7$ range.

convective mantle, where deuterium burning takes place. The efficiency of the magnetic dynamo and the X-ray activity level of the star strongly depend on the precise boundary between these two regions, and this boundary changes with the age and accretion history of the PMS phase. For even more massive stars, the mechanism for the production of X-rays changes drastically.

4.3. X-Ray Activity in Class III and Class II Members

It is still debated whether the X-ray activity in PMS stars can be affected by the presence of a circumstellar disk. Several authors have compared the X-ray luminosity of Class III and Class II members of young clusters, and the general picture remains unclear. In some cases, such as Chamaleon I (Feigelson et al. 1993), ρ Ophiuchi (Casanova et al. 1995), and IC348 (Preibisch & Zinnecker 2002), the same level of X-ray activity in disk-less and disk-bearing members has been found; while in other clusters, such as the Taurus–Auriga region (Stelzer & Neuhäuser 2001), NGC 1893 (Caramazza et al. 2012), and NGC 2264 (Flaccomio et al. 2006), the X-ray luminosity of Class II objects is significantly lower than that in Class III stars. In the ONC the first attempt to find any difference in X-ray activity between these two classes of PMS stars was made by Gagne et al. (1995), who found no significant difference. Later, Flaccomio et al. (2003) discovered a different emission level in accreting and non-accreting stars in Orion. This result was reinforced by Preibisch & Feigelson (2005), taking advantage of the completeness of the member selection with the deep COUP data. These authors found no difference in X-ray emission between stars with and without infrared excesses, detected with a diagnostic based on the L photometric band, but they found a significant difference between non-accreting and accreting stars selected using the Ca II line emission. Their finding suggests that the effects on the X-ray activity in disk-bearing stars are not due to the presence of the disk itself, but due to active accretion. In fact, in the ONC study of Prisinzano et al. (2008), where the disk-bearing stars have been selected by means of their infrared excesses, the level of X-ray emission in Class II and Class III stars is only marginally different.

The present study of the stellar population of M16 can help shed some light on the effects of the circumstellar disk in the X-ray emission in young stars, taking advantage of the accurate selection of both Class II and Class III members. However, a reliable comparison between the X-ray luminosity distributions of Class II and Class III objects can be attempted only if the two samples are complete. The Class II sample (219 stars) can be easily completed using the upper limits of L_X of the undetected Class II objects (see Section 2.5). These upper limits, together with the X-ray luminosity of detected Class II and Class III objects, are shown in the left panel of Figure 9 as a function of stellar mass.

We cannot complete the Class III sample with the same approach adopted for Class II stars, since we do not have a representative sample defined independently of X-ray information. However, we can estimate the fraction of Class III members with X-ray emission below our completeness limit using the COUP data of Orion. Our sample of Class III objects, as well as the Class II, is more massive than $0.2\,M_\odot$ (Guarcello et al. 2010b), and in Orion 15% of the Class III objects with $M > 0.2\,M_\odot$ have $\log(L_X) < 30\,\mathrm{erg\,s^{-1}}$. Given the similarities between the X-ray properties of the two clusters, we can suppose that this is also valid for M16, i.e., that the undetected Class III stars more massive than $0.2\,M_\odot$ are 15% of the detections (124 sources). Regarding their upper L_X limit, since our aim is to verify whether the X-ray activity in Class III sources is higher than that in Class II objects, we can consider the most conservative case, resulting in the lowest L_X distribution for Class III stars: that the upper limit of the X-ray luminosity of the missing Class III stars is equal to the lowest L_X measured for Class III objects in the COUP survey (Getman et al. 2005), equal to $\log(L_X) = 27.89\,\mathrm{erg\,s^{-1}}$. We then calculated the XLFs for the "completed" samples of Class III (detected Class III sources plus 124 sources with $\log(L_X) = 27.89\,\mathrm{erg\,s^{-1}}$) and Class II

objects (detected Class II objects plus the upper limits of the undetected Class II objects), which are shown in the right panel of Figure 9. The emission level of the completed sample of Class II objects is evidently lower than that of the Class III, and we have verified with the ASURV[9] (Feigelson & Nelson 1985) statistical package that the probability that the two XLFs are drawn from the same parent distribution is null. In the left panel, a few sources with $\log(L_X) = 29.5\,\mathrm{erg\,s^{-1}}$ are present (fainter than our detection limit). They are low significance sources, whose luminosity has been inferred directly from their count rates. In conclusion, in M16 the level of X-ray emission is higher in Class III objects than in disk-bearing stars, supporting the idea that the presence of a disk results in lower X-ray activity. We cannot discern between accreting and non-accreting disks, but it can be expected that, since the average age of the M16 population is ∼1 Myr (Guarcello et al. 2007), a large fraction of stars with disks are still actively accreting.

There is more than one hypothesis to explain the observed X-ray emission level lower in Class II than in Class III stars. The accreting material, for instance, could be responsible for a higher absorption in disk-bearing objects. In fact, the correction we made for the extinction cannot be completely appropriate for disk-bearing stars. For these objects, it would be more appropriate to use an extinction model that takes into account the presence of both interstellar and circumstellar obscuring material (E. Flaccomio et al., in preparation). It is also possible that the accreting material deforms the large-scale stellar magnetic field (Romanova et al. 2004) or that it increases the gas density in the magnetic loops around the stars, resulting in less efficient heating of the material by the energy released during flares (Preibisch & Feigelson 2005), even if this would require a fraction of the stellar surface covered by hot spots larger than the typical values observed in CTTS (Muzerolle et al. 2001). The last possibility is that the accretion phenomenon changes the internal structure of the star, as pointed out by Wuchterl & Tscharnuter (2003), who found that even with small accretion rates the central star is no longer fully convective. A different hypothesis is that the presence of the accreting inner disk is not the cause of the lower X-ray activity but a consequence, since, as discovered by Drake et al. (2009), a high X-ray flux emitted by the central star can enhance the photoevaporation of the disk.

Only one Class I object has been detected in X-rays. Its position is $\alpha = 20{:}33{:}51.237$ and $\delta = +41{:}25{:}10.68$, and it has only IRAC and *Chandra* detections with a high X-ray luminosity $\log(L_X) = 31.49\,\mathrm{erg\,s^{-1}}$ derived from the spectral fit with a one-temperature thermal model. This source lies in the embedded cluster in the *ne-field*, and it is not surprising that it has a very high extinction ($N_\mathrm{H} = 48.0 \times 10^{22}\,\mathrm{cm^{-2}}$, corresponding to $A_V = 60.8^m$). The X-ray luminosity of this source is about half an order of magnitude higher than that of the brightest Class I objects in Orion (Prisinzano et al. 2008), but a similar embedded object has been identified in M17 (Broos et al. 2007). However, neither the IRAC nor the X-ray data allow us to discard the possibility that this source is a background AGN, whose locus in the IRAC color–color diagram (used to classify the selected disk-bearing stars) roughly coincides with that of Class I objects. The fit of the source spectrum with a power-law model is statistically acceptable and the photon index we obtained is equal to 2.03, compatible with typical values of AGN spectra. The only valid argument against the extragalactic nature of this source is its spatial correspondence with the embedded NE cluster.

[9] Astronomy Survival Analysis, http://www.astro.psu.edu/statcodes.

5. X-RAY EMISSION IN HIGH-MASS STARS

NGC 6611 is a young massive cluster comprising several massive stars. In the ACIS fields of view fall 13 O stars and 80 B stars, with one of the few O4–O5 stars known in our Galaxy with a mass of 75–80 $M_\odot$ (W205), and two known O binary systems (W175, an O8.5V+O5V system, Bosch et al. 1999; W205 itself, O4V+O7.5V, Sana et al. 2009). In our observations, we detected 85% of the O stars (11/13), 48% of the B0–B2 stars (24/54), and 19% of the B3–B9 stars (7/36), among which there are two giant stars accounting for a good sample of stars to study the mechanisms for the production of X-rays in young massive stars. In this section, we use the stellar nomenclature by de Winter et al. (1997).

The X-ray properties of the detected OB stars in NGC 6611 are summarized in Table 1. For those stars observed in two observations (in all cases in the *c-field* and *e-field*), the table shows two values of N_H, kT, and L_X, corresponding to the *c-field* and *e-field*. The variability diagnosis comes from the K-S test on the light curve provided by AE (see the Appendix for details); the spectral classification is taken from Hillenbrand et al. (1993), Evans et al. (2005), Dufton et al. (2006), and Martayan et al. (2008), while the binarity information is from Duchêne et al. (2001), Herbig & Dahm (2001), Gvaramadze & Bomans (2008), and Sana et al. (2009).

5.1. X-Ray Emission from the O Stars

Generally, O and late-B stars are sources of soft ($kT \sim 0.5$ keV) X-rays, thought to be produced in a myriad of small shocks in their radiatively accelerated winds (Owocki & Cohen 1999). This emission is usually slowly variable, and, since the wind intensity scales with L_bol, X-ray emission also scales with L_bol, usually approximately as $L_X = 10^{-7} \times L_\mathrm{bol} = 10^{31}$–$10^{33}\,\mathrm{erg\,s^{-1}}$ (Harnden et al. 1979; Pallavicini et al. 1981). However, a large scatter is usually observed, mostly due to a wide range of shock filling factors and binarity. Usually, a thermal emission spectrum observed in an OB star with $kT = 0.5$–0.7 keV and with a constant or slightly variable light curve is a signature that the X-ray emission is produced by the self-shocked wind. In some cases, however, an intermediate/hard component in the X-ray emission from O stars has also been observed: a moderate hard component ($kT = 2$–3 keV) rotationally modulated or with rapid variability (Stelzer et al. 2005) or a very hard thermal component due to shocks in the magnetically confined wind in the stellar equatorial plane in stars with strong magnetic dipole (Babel & Montmerle 1997); wind–wind collision in close massive binaries (Pollock et al. 2005), which can also be a source of soft X-ray emission (Gagné et al. 2011); or a hard non-thermal component caused by inverse Compton scattering of UV stellar photons by relativistic charged particles in the stellar wind (Chen & White 1991).

As listed in Table 1, all the O stars in NGC 6611 have soft spectra (with one exception that will be discussed later), suggesting that in M16 the shocked wind emission is the only mechanism producing X-rays in the O stars. Figure 10 shows the $\log(L_X)$ versus $\log(L_\mathrm{bol})$ relation for the OB stars in NGC 6611. The best linear fit for stars with $L_\mathrm{bol} > 10^{37}\,\mathrm{erg\,s^{-1}}$ (the sample of B stars with $\log(L_\mathrm{bol}) < 37\,\mathrm{erg\,s^{-1}}$ is strongly incomplete) gives a slope of 0.7×10^{-7} (dashed line), similar to the $L_X \sim 10^{-7} \cdot L_\mathrm{bol}$ relation (represented by the solid line)

Table 1
X-Ray Properties of the OB Stars

ID	Net Counts	Results[a]	N_H ($\times 10^{22}$ cm^{-2})[b]	kT (keV)[b]	kT_2[b]	log(L_X) (erg s^{-1})[b]	log(L_{bol}/L_{sun})	Variable[c]	Spectral Type	Binary
W205	754.7	*F*	0.54	0.63		32.17	5.58	Y	O4III,O4V,O5	Y
W175	1258.0	*F*	0.78	0.37	3.62	32.65	5.49	Y	O5V+O8.5V	Y
W197	1041.0	*Q*	0.05	0.93		31.47	5.23	Y	O7V	Y
W222	176.2	*F*	1.69	0.36		32.09	5.14	N	O7V,O7III	
W246	272.2	*F*	0.67	0.53		31.70	5.62	N	O7II	
W401	413.3	*F*	0.15	0.54		31.26	4.86	N	O8.5V	
W161	208.6	*Q*	1.24	0.34		32.33	4.86	N	O8.5V	?
W166	151.4	*F*	0.45	0.54		31.06	4.82	N	O8.5,O9V	
W314	99.6	*F*	0.19	0.62		30.64	4.52	N	O9V,B0V	Y
W280	60.9	*F*	0.51	0.59		31.05	4.68	Y	O9.5Vn	
W367	119.6	*F*	0.01	0.44		30.59	5.15	N	O9.7III,O9.5V	
W188	36.6	*F*	0.74	0.97		30.55	4.26	N	B0V	Y
W259	21.5	*N*	0.14	10.0		30.06	4.04	Y	B0.5V	
W150	19.91	*Q*	0.05	1.01		29.62	4.04	Y	B0.5V	
W469	12.6	*Q*	1.12	0.70		30.51	4.04	?	B0.5Vn	?
W351	15.7	*Q*	0.05	2.90		29.76	3.82	N	B1V	
W343	33.6, 30.5	*F*	0.09, 0.67	22.3, 2.62		30.24, 30.30	3.82	Y	B1V	Y
W25	65.5	*F*	0.83	1.49		30.82	3.93	N	B1V,B0.5V	Y
W125	29.6	*Q*	0.33	1.67		30.17	3.82	Y	B1.5V,B1V	Y
W207	196.0	*F*	0.51	1.95		31.07	3.82	Y	B1V	
W231	156.3	*F*	0.49	2.97		30.99	3.82	Y	B1V	
W254	3.58	*Q*	0.19	0.30		29.09	3.82	?	B1V	Y
W444	17.7	*Q*	0.09	2.08		30.02	3.63	?	B1V, B1.5V	?
W296	42.3	*F*	0.17	1.88		30.23	3.57	N	B1.5V	
W601	31.3	*F*	0.11	1.72		30.22	3.57	Y	B1.5V	
W421	93.5, 118.6	*F*	0.48, 1.67	2.64, 1.15		30.81, 31.30	3.57	N	B1.5:V	
W80	42.1	*F*	0.09	4.14		30.33	3.57	N	B1V,B2V	
W300	14.5	*Q*	0.05	1.01		29.54	3.45	N	B2V,B1.5V	
W227	140.3	*F*	1.58	0.44	38.61	31.65	3.45	Y	B2V,B1.5V	Y
W269	16.7	*Q*	1.64	0.62		30.89	3.45	N	B2V,B1.5V	
W228	195.8	*F*	0.68	4.70		31.21	3.32	Y	B2V	
W251	50.45	*F*	0.35	2.17		30.44	3.32	Y	B2V	
W607	145.9	*Q*	0.43	0.43		31.04	2.81	N	B3V	
W371	225.6	*F*	0.44	9.05		31.23	3.17	Y	B4V,B0.5V	
W336	8.7	*Q*	0.12	0.3		29.40	3.32	?	B5III	
W276	93.76	*F*	0.25	2.93		30.71	2.14	N	B6V	
W364	7.6	*Q*	0.51	2.25		29.88	2.05	?	B7V	Y
W243	33.6	*F*	1.37	0.84		30.74	2.01	Y	B4V,B8V	Y
W221	64.1	*F*	0.51	2.00		30.62	1.71	N	B8V	
W322	5.7	*Q*	0.16	0.3		29.19	1.95	?	B8V	
W400	83.9	*F*	0.20	1.67		30.60		N	B9III,B8IV	Y
W310	110.5	*F*	0.35	0.69		30.84		N	B+G	Y

Notes.
[a] *F* spectral fit, *Q* quantiles, *C* conversion from the count rate.
[b] Two values if the star has been observed twice.
[c] ? no light curve.

typical of the shocked wind emission, as found first by Harnden et al. (1979) and Pallavicini et al. (1981) and then observed in other massive star-forming regions (i.e., in the Carina region; Nazé et al. 2011).

A significant level of hard emission should be expected in principle from the O4V and O7.5V binary system W205 from the collision of the intense stellar wind emitted from the two components (expected to be $\sim 2.0 \times 10^{-6}\,M_\odot\,\mathrm{yr}^{-1}$ and $\sim 0.35 \times 10^{-6}\,M_\odot\,\mathrm{yr}^{-1}$; Smith 2006), but the separation between the two stars is too large (Sana et al. 2009 reported a rotation period of hundreds of years) to expect a significant wind+wind X-ray emission.

Only for W175 does the spectral fit suggest the presence of a possible hard component. This system is composed of an O8.5V and an O5V stars, with a third intermediate mass (spectral types A–F) component reported by Duchêne et al. (2001). The separation between the two more massive components is about 1200 AU (Sana et al. 2009). As expected, W175 is very bright in our *Chandra* observations, with 1258 net counts and $\log(L_X) = 32.65$ erg s^{-1}. The spectral fit with abundances fixed at standard values is very poor, with $\chi^2_\nu = 2.06$ indicating a statistically unacceptable fit. An acceptable spectral fit ($\chi^2_\nu = 0.86$) was instead obtained adopting a two-temperature thermal model with abundances for iron and oxygen allowed to vary. The values of N_H, kT, and L_X of W175 obtained with this fit are reported in Table 1, and the abundances found are $O = 2.3 \pm 0.7\,O_\odot$ and $Fe = 0.7 \pm 0.2\,Fe_\odot$. In O stars a subsolar abundance of iron can be expected, as predicted, for example, by the model developed by Zhekov & Palla (2007), but in the case of W175 the iron abundance is only marginally subsolar. This spectral fit

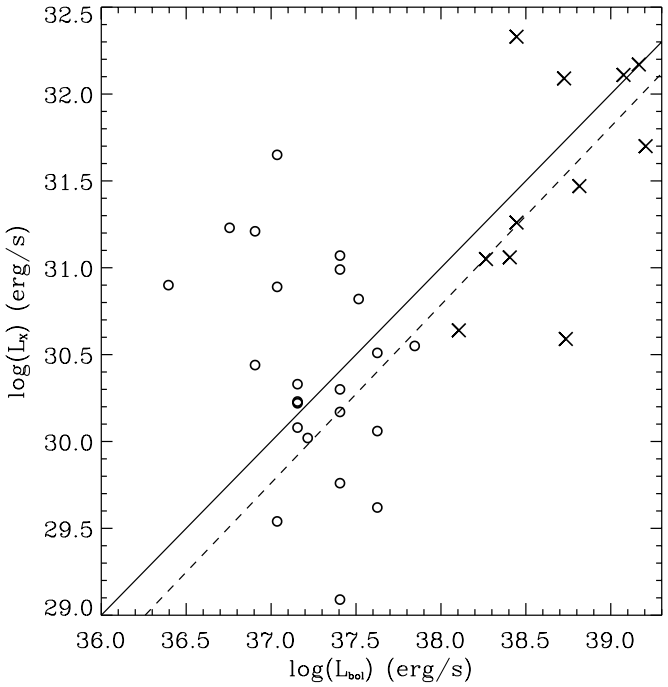

Figure 10. $\log(L_X)$ vs. $\log(L_{\rm bol})$ for the detected O (crosses) and B (circles) stars in NGC 6611. The dashed line is the best-fit line calculated for stars with $\log(L_{\rm bol}) > 37\,{\rm erg\,s^{-1}}$; the solid line is the typical $L_X \sim 10^{-7} \cdot L_{\rm bol}$ relation.

suggests the presence of a hard component with a temperature $kT = 4 \pm 2$ keV, even if the emission measure of this hot plasma is more than 20 times smaller than that of the cold component, which can be produced in the wind-colliding zone such as those observed in other similar systems (i.e., HD 93129A; Gagné et al. 2011). Figure 11 shows the two-temperature thermal plasma model fitted to the W175 spectrum.

5.2. X-Ray Emission from B and Intermediate-Mass Stars

In the sample of early-B stars of NGC 6611, the ratio of bolometric flux emitted in X-ray ranges from $-5.4 \leqslant \log(L_X/L_{\rm bol}) \leqslant -8.5$. This large scatter is related to the variety of mechanisms for X-ray production operating in this family of stars. Among these B stars, 10 have $kT < 1$ keV and a constant light curve, according to the K-S test performed by AE. Their X-ray emission is then typical of shocked wind emission. On the other hand, 21 early B-stars have a plasma temperature $kT > 1$ keV, with 6 of them showing very hard spectra, with $kT > 3$ keV. For the B stars with plasma temperature $kT > 1$ keV, the K-S test cannot help to discern between the possibility that the hard emission is due to an unresolved low-mass companion or to the action of one of the mechanisms described above. However, among the six stars with $kT > 3$ keV, five are not spectroscopically classified as close binary systems; for these, the hard X-ray emission cannot be produced by colliding winds. Their light curves produced by AE suggest some flaring activity that will be studied in detail in a forthcoming paper. This emission can come from a low-mass unresolved companion in a wide orbit observed during a flaring activity or from the B stars themselves, since, as proposed by Feigelson et al. (2002), magnetic reconnection events can take place on the surface of young B stars.

One peculiar case is W601. This B1.5V star has been suggested to be very young (0.016 Myr) and in a transition phase between the Class II and the MS phases, with a P Cygni

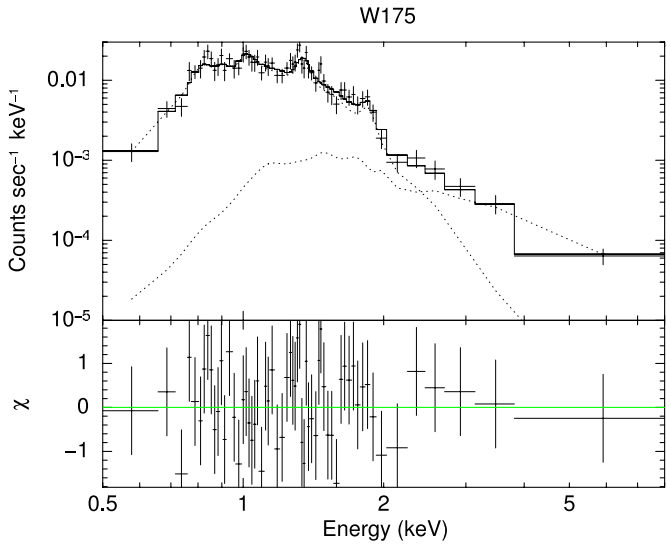

Figure 11. Thermal plasma model for W175. The two-temperature components are shown as dotted lines.

(A color version of this figure is available in the online journal.)

like H_α line typical of the presence of outflow/infall activity (Martayan et al. 2008). This star has been studied in detail by Alecian et al. (2008), who found an accretion rate equal to $10^{-4}\,M_\odot \cdot {\rm yr}^{-1}$, a rotational velocity of $190 \pm 10\,{\rm Km\,s^{-1}}$, and an intense mean magnetic field equal to 3 kG, classifying it as a Herbig Be star. With these characteristics, it is not surprising that we detected an intermediately hard component in the W601 spectrum ($kT = 1.72$ keV). The K-S probability that the light curve is constant is high (0.96).

As expected, the fraction of detected sources in the A to late-B range of spectral classes is very low: 19% of late-B stars and 10% of the A–F stars, with $\log(L_X) < 30.4\,{\rm erg\,s^{-1}}$, consistent with emission from a low-mass companion following the L_X versus mass relation shown in Figure 8. Evidence that the X-ray emission detected from A-late B stars is due to a low-mass companion has been obtained by De Rosa et al. (2011), who found that multiplicity in a sample of X-ray-detected intermediate-mass stars is about four times higher than in a control sample of stars.

6. X-RAY PROPERTIES OF THE POPULATION OF SELECTED REGIONS OF M16

In this section, we analyze the X-ray properties of the YSO populations of selected regions of M16 with different characteristics. Figure 12 shows these regions on an IRAC [8.0] image. In the following discussion, the median age of the members falling in each region are taken from Guarcello et al. (2010b), which also includes a detailed description of the evolutionary status of the sources falling in some of these regions.

6.1. The Central Cavity

The central cavity contains the core of NGC 6611, with almost all the OB stars discussed in Section 5 and a rich YSO population (385 members detected in X-rays, among which 21% have a disk) with a median age of 1 Myr. This region has the highest fraction of members with disks among all the regions analyzed in this section. The median $N_{\rm H}$ of the X-ray members is $0.52 \times 10^{22}\,{\rm cm^{-2}}$, corresponding to an

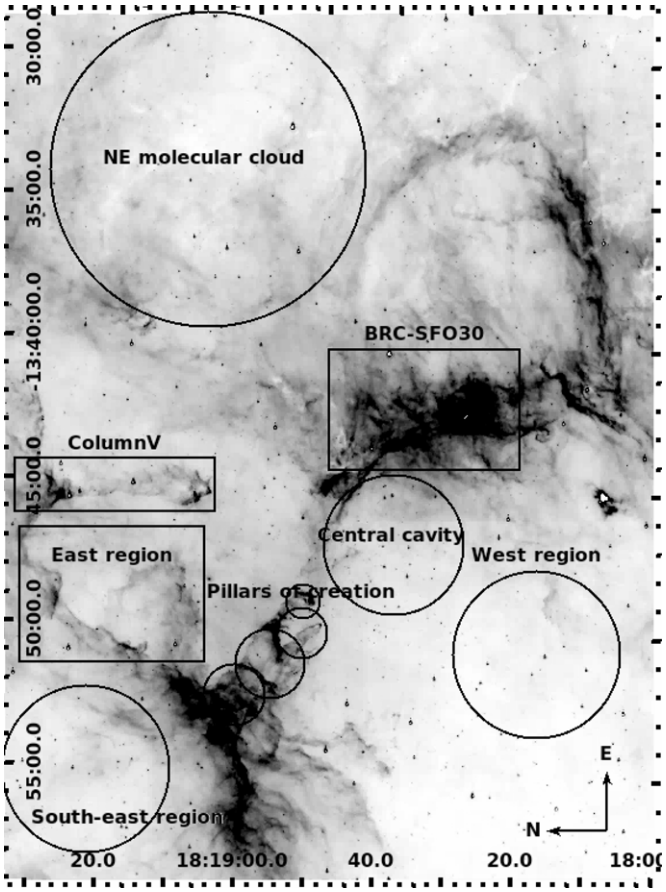

Figure 12. IRAC [8.0] image of M16 marked with all the regions whose populations are analyzed in Section 6.

extinction of $A_V = 2.91^m$, slightly larger than that estimated by Guarcello et al. (2007) from the optical color–magnitude diagrams ($A_V = 2.7^m$); the median plasma temperature is $kT = 1.95$ keV, lower than the median value of the whole population. In the central cavity there is a significant population of candidate background sources (45 sources, 10% of the total number of X-ray sources in this field). It is likely that most of these are really background contaminants, since we do not expect a large embedded population in this field where the molecular cloud has been cleared by the energetic radiation from the OB stars lying in this region.

6.2. The Pillars of Creation

There are 33 members of the Pillars of Creation (8 with disks), with an age of about 2–3 Myr old in the bottom of the pillar, in the southeast, getting younger in the direction of the tip of the pillars. The median absorption of the X-ray sources falling in this region is typical of the cluster ($N_{\rm H} = 0.45 \times 10^{22}$ cm^{-2}), suggesting that almost all these sources belong to the cluster but they are not physically associated with the pillars. The median plasma temperature is $kT = 2.03$ keV, lower than the median of the members of the whole cluster. Three X-ray sources are associated with the tip of the largest pillar, called Pillar 1, where a protostar with a mass of 4–5 $M_\odot$ and an intense infrared excess has been found (McCaughrean & Andersen 2002). One (at $\alpha = 18{:}18{:}50.88$ and $\delta = -13{:}48{:}43.48$) has been classified as a foreground source, and its $N_{\rm H}$, derived from the quantile analysis, is compatible with this classification ($N_{\rm H} = 2 \times 10^{19}$ cm^{-2}, corresponding to an $A_V = 0.01^m$). The second source is a disk-less member located at $\alpha = 18{:}18{:}49.78$ and $\delta = -13{:}48{:}56.2$. It has a spectrum fitted with a one-temperature thermal plasma model, with $kT = 1.71$ keV and $N_{\rm H} = 0.43 \times 10^{22}$ cm^{-2}, which corresponds to the average extinction of the cluster, suggesting that this source is not embedded in the pillar. The only likely X-ray counterpart of the protostar in the tip of the pillar is at $\alpha = 18{:}18{:}50.31$ and $\delta = -13{:}48{:}54.31$, with 103 net counts, an absorption $N_{\rm H} = 3.89 \times 10^{22}$ cm^{-2}, corresponding to an $A_V = 21.7^m$, and a plasma temperature of $kT = 10.89$ keV and $\log(L_X) = 31.69$ erg s^{-1}, suggesting an embedded very active young star with an X-ray thermal spectrum. The X-ray counterpart of this protostar has already been identified by Linsky et al. (2007).

6.3. The Column V

In the other pillar of M16, *Column V*, fall 32 members (6 with a disk) with an age of about 1 Myr. Their median absorption is $N_{\rm H} = 0.95 \times 10^{22}$ cm^{-2}, twice that of the central cavity, with the most obscured sources at the bottom of the pillar. The median value for the plasma temperature is $kT = 2.18$ keV. Meaburn & Walsh (1986) discovered a bright Herbig–Haro object in the tip of Column V. We detected one X-ray source at less than 1″ away from it, at $\alpha = 18{:}19{:}04.65$ and $\delta = -13{:}45{:}32.31$. The quantile analysis revealed a plasma temperature of $kT = 3.4$ keV, an intermediate absorption ($N_{\rm H} = 0.3 \times 10^{22}$ cm^{-2}), and an X-ray luminosity $L_X = 10^{30.1}$ erg s^{-1}. Another candidate embedded protostar of Column V detected in X-rays at $\alpha = 18{:}19{:}07.08$ and $\delta = -13{:}45{:}22.54$ can be associated with water masers identified by Healy et al. (2004). This source is without a stellar counterpart in our catalog. It has been observed both in the *c-field* (32.7 net counts, $\log(L_X) = 30.6$ erg s^{-1}, and a spectrum fitted by a power law) and the *e-field* (11.8 net counts).

6.4. The Bright Rimmed Cloud SFO30

Another region rich in cluster members is BRC SFO30, with 85 members (6 with a disk) detected in X-rays. In the optical and infrared diagrams, these sources are largely extinct ($A_V > 5^m$). The median absorption ($N_{\rm H} = 1.16 \times 10^{22}$ cm^{-2}) is similar to that of the sources falling in Column V, with a median plasma temperature of $kT = 2.67$ keV. The distribution of plasma temperature of these stars, however, has a very hot tail, with the 66% terzile at $kT = 5.33$ keV. Considering all the X-ray sources falling in this region, there is the largest fraction of candidate members without a disk and the lowest of candidate background sources. Since, from infrared studies (Indebetouw et al. 2007; Guarcello et al. 2009) and detection of water masers (Healy et al. 2004), a population of embedded protostars is expected to fall in this region, it is possible that the extinction here is high enough to efficiently absorb all the background sources or that these protostars are not yet X-ray active (the population of this region is on average younger than 1 Myr).

6.5. The North East Embedded Cluster

The most extinguished region is the NE molecular cloud, where a young embedded cluster lies (Indebetouw et al. 2007; Guarcello et al. 2009). This region has the highest fraction of X-ray sources without stellar counterparts (82 sources, 52% of all X-ray sources falling in this region). Among the 70 candidate YSOs in this region, 12 have a disk and are classified as embedded YSOs from their IRAC colors (among them are also the Class I sources detected in X-ray discussed in Section 4). It is not surprising that this is the region with the highest median

absorption, with $N_{\rm H} = 1.92 \times 10^{22}\,{\rm cm}^{-2}$, which is four times larger than the value in the central cavity and corresponds to an $A_V = 10.7^m$.

6.6. The Other Regions

The remaining regions are the poorest in candidate cluster members. In the east region the 60 members detected in X-rays (12 with a disk) are older than 1 Myr, with a median absorption similar to the central cavity ($N_{\rm H} = 0.65 \times 10^{22}\,{\rm cm}^{-2}$) and a median plasma temperature of $kT = 2.5\,{\rm keV}$. The members detected in X-ray falling in the west region (25 sources, none with a disk) have similar ages, an absorption lower than the members in the central cavity (median value $N_{\rm H} = 0.33 \times 10^{22}\,{\rm cm}^{-2}$), and a median plasma temperature of $kT = 2.45\,{\rm keV}$. The southeast region contains the oldest X-ray-detected cluster members (12 sources, one with a disk, with a median age of about 3 Myr), with the lowest median plasma temperature ($kT = 1.72\,{\rm keV}$) and a median absorption of the candidate members detected in X-rays smaller than that of the central cavity ($N_{\rm H} = 0.36 \times 10^{22}\,{\rm cm}^{-2}$).

7. SUMMARY AND CONCLUSIONS

In this paper, we analyze three 80 ks *Chandra*/ACIS-I observations of the Eagle Nebula: one archival centered on the young open cluster NGC 6611 in the center of the nebula, one centered on the evaporating pillars named "Column V," and one in the northeast region centered on an embedded cluster of very YSOs. The final catalog of the X-ray sources amounts to 1755 entries, classified from their photometric properties as "disk-bearing cluster members" (219 sources), "disk-less cluster members" (964), "foreground sources" (76), and "background sources" (504).

Spectral properties and X-ray luminosities have been derived from spectral fitting and analysis of the photon energy quantiles. Considering all the cluster members detected in X-ray, we found a median $N_{\rm H} = 0.640 \times 10^{22}\,{\rm cm}^{-2}$, corresponding to a median extinction of $A_V = 3.6^m$, and a median $kT = 2.13\,{\rm keV}$. The median $N_{\rm H}$ is three times larger in the northeast field with respect to the central field where NGC 6611 has cleared most of the parental cloud.

We compared the X-ray properties of M16 members and those in the ONC, which is the best-characterized sample of X-ray sources in a young cluster. The XLF has similar slope (a power law with $\Gamma = -0.85 \pm 0.09$) in a range of luminosities $\log(L_X) > 30\,{\rm erg\,s}^{-1}$, which is the completeness limit of our observations. This allowed us to estimate that the total population of M16 should be about 2700 members. Also, the slope of the L_X versus mass function is similar to that in Orion for masses smaller than $0.8\,M_\odot$, while for larger masses the distribution is flat around $\log(L_X) = 30.72\,{\rm erg\,s}^{-1}$, with a large spread. These analogies support the universality of the XLFs and the L_x versus mass relation for clusters younger than 5 Myr.

Our study supports the evidence that the X-ray activity in disk-bearing stars is less intense than that in disk-less stars of similar mass. This result also has been obtained in other young clusters, while in some other cases no dependence with the presence of disk in the X-ray activity has been observed. The present study of M16 supports, then, the idea that the presence of a circumstellar disk, likely due to the accretion process, affects the coronal activity in the hosting star.

We took advantage of the large population of massive stars detected in X-rays (11 O stars, a 85% detection rate, and 31 B stars, 39%) to study the mechanism for the production of X-rays in such massive stars. All the O stars but one have soft spectra without a hard component and have constant light curves, suggesting that the X-ray photons are produced by shocks propagating in the stellar wind. A hard component has been detected only in one case (a triple system with two O stars and an A–F star), but it is only marginally significant, contributing less than 5% of the total spectrum.

The sample of detected B stars is more heterogeneous, with 10 sources with soft spectra typical of wind emission, and 21 with $kT > 1\,{\rm keV}$. For these latter sources, it not possible to discern the possibility that some mechanism for the production of hard X-ray photons is at work or the emission is due to unresolved companions. However, the binarity of the massive stars of M16 has been studied by several authors, and most of these stars do not show evidence for such companions. In particular, among the six B stars with $kT > 3\,{\rm keV}$, only one is a binary system, but with 2 B stars, and all of them seem to have flares in their light curves. This result suggests that in these young massive stars some magnetic reconnection events can occur on the stellar surface.

Finally, the X-ray properties of the sources in relevant regions of M16, such as the central cavity and the Pillars of Creation, have been discussed to analyze the different properties of the M16 population in different locations of the nebula.

We thank the anonymous referee for useful comments and suggestions. This work is based on observations performed with *Chandra*/ACIS-I. M. G. G. was supported by Chandra Grant GO0-11040X. J. J. D. was supported by the NASA contract NAS8-39073 to the Chandra X-ray Center and thanks the Director, H. Tananbaum, for continuing advice and support. G.M., S.S., M.C., and L.P. were supported by the contract PRIN-INAF 2009.

APPENDIX

SOURCE CATALOG

Information about the X-ray sources of M16 analyzed in this work is available in an online catalog. The catalog is not shown here because of the large number of columns. In the following, we describe the data available in the catalog:

1. $RA, decl.$: source position in J2000.
2. $\sigma_{\rm pos}$: the uncertainty on source position found by AE.
3. θ: the source off-axis angle.
4. *PBS*: the probability associated with the null-hypothesis that there is not a real source associated with the position. Only 21 sources have a *PBS* value larger than the threshold of 0.1 typically used with AE.
5. $Sgnf$: photometric significance computed as the ratio between the net counts in 0.5–8 keV on the upper error of net counts.
6. *Status*: class of the source, based on its optical/infrared properties (disk-bearing members, disk-less members, foreground source, and background source).
7. $Cnts$: the total number of counts associated with the source in the whole energy band (0.5–8 keV).
8. Bkg_cnts: the observed background counts associated with the source in the whole energy band (0.5–8 keV).
9. Net_cnts: the net counts associated with the source in the whole energy band (0.5–8 keV).
10. *PSF_frac*: the fraction of the PSF at 1.497 keV corresponding to the extraction region.

11. $medE$: the median photon energy in keV.
12. $N_{\rm H}$: the value of the hydrogen column density in the direction of the source, in units of 10^{22} cm^{-2}. This value is estimated either from the spectral fitting or quantile analysis as described in Section 3, with errors.
13. kT: temperature of the emitting plasma, in keV. This value is estimated either from the spectral fitting or quantile analysis as described in Section 3, with errors.
14. kT_2: second temperature of the emitting plasma, in keV, for the sources whose spectra are well fitted by a thermal two-temperature plasma model, with errors.
15. P_0: index of the power law for the sources whose spectrum is best fitted by a power-law model.
16. L_X: the adopted X-ray luminosity for the source. See Section 4 for details on how L_X is determined, with errors.
17. $Model$: the model used to fit the source spectrum (thermal, 2T thermal, power law). See Section 2.3.
18. $P_{\rm K-S}$: probability based on the K-S statistic with the null hypothesis that the source is not variable (in the total band). The classification suggested by the AE manual is: no evidence for variability ($0.05 < P_{\rm K-S}$); possibly variable ($0.005 < P_{\rm K-S} < 0.05$); definitely variable ($P_{\rm K-S} < 0.005$).

All the information, but the position, *PBS* and *Status*, are provided for all three observations, sorted in alphabetical order (*c-field*, *e-field*, and *ne-field*), for a total of 63 columns.

REFERENCES

Alecian, E., Wade, G. A., Catala, C., et al. 2008, A&A, 481, L99
Babel, J., & Montmerle, T. 1997, ApJ, 485, L29
Bosch, G. L., Morrell, N. I., & Niemela, V. S. 1999, RevMexAA, 35, 85
Brandt, W. N., Alexander, D. M., Hornschemeier, A. E., et al. 2001, AJ, 122, 2810
Broos, P. S., Feigelson, E. D., Townsley, L. K., et al. 2007, ApJS, 169, 353
Broos, P. S., Townsley, L. K., Feigelson, E. D., et al. 2010, ApJ, 714, 1582
Caramazza, M., Flaccomio, E., Micela, G., et al. 2007, A&A, 471, 645
Caramazza, M., Micela, G., Prisinzano, L., et al. 2012, A&A, 539, A74
Casanova, S., Montmerle, T., Feigelson, E. D., & Andre, P. 1995, ApJ, 439, 752
Chen, W., & White, R. L. 1991, ApJ, 366, 512
Damiani, F., Maggio, A., Micela, G., & Sciortino, S. 1997, ApJ, 483, 350
De Rosa, R. J., Bulger, J., Patience, J., et al. 2011, MNRAS, 415, 854
de Winter, D., Koulis, C., The, P. S., et al. 1997, A&AS, 121, 223
Drake, J., Wright, N., & The Chandra Cyg Ob2 Team. 2009, in Chandra's First Decade of Discovery, ed. S. Wolk, A. Fruscione, & D. Swartz, (http://cxc.harvard.edu/ChandraDecade/proceedings/stars_formation.html#abs1.3)
Drake, J. J., Peres, G., Orlando, S., Laming, J. M., & Maggio, A. 2000, ApJ, 545, 1074
Duchêne, G., Simon, T., Eislöffel, J., & Bouvier, J. 2001, A&A, 379, 147
Dufton, P. L., Smartt, S. J., Lee, J. K., et al. 2006, A&A, 457, 265
Evans, C. J., Smartt, S. J., Lee, J.-K., et al. 2005, A&A, 437, 467
Feigelson, E. D., Broos, P., Gaffney, J. A., III, et al. 2002, ApJ, 574, 258
Feigelson, E. D., Casanova, S., Montmerle, T., & Guibert, J. 1993, ApJ, 416, 623
Feigelson, E. D., & Decampli, W. M. 1981, ApJ, 243, L89
Feigelson, E. D., Gaffney, J. A., III, Garmire, G., Hillenbrand, L. A., & Townsley, L. 2003, ApJ, 584, 911
Feigelson, E. D., Getman, K., Townsley, L., et al. 2005, ApJS, 160, 379
Feigelson, E. D., & Nelson, P. I. 1985, ApJ, 293, 192
Flaccomio, E., Damiani, F., Micela, G., et al. 2003, ApJ, 582, 398
Flaccomio, E., Micela, G., & Sciortino, S. 2006, A&A, 455, 903
Flagey, N., Boulanger, F., Noriega-Crespo, A., et al. 2011, A&A, 531, A51
Gagne, M., Caillault, J.-P., & Stauffer, J. R. 1995, ApJ, 445, 280
Gagné, M., Fehon, G., Savoy, M. R., et al. 2011, ApJS, 194, 5
Getman, K. V., Flaccomio, E., Broos, P. S., et al. 2005, ApJS, 160, 319
Guarcello, M. G., Damiani, F., Micela, G., et al. 2010a, A&A, 521, A18
Guarcello, M. G., Micela, G., Damiani, F., et al. 2009, A&A, 496, 453
Guarcello, M. G., Micela, G., Peres, G., Prisinzano, L., & Sciortino, S. 2010b, A&A, 521, A61
Guarcello, M. G., Prisinzano, L., Micela, G., et al. 2007, A&A, 462, 245
Gvaramadze, V. V., & Bomans, D. J. 2008, A&A, 490, 1071
Harnden, F. R., Jr., Branduardi, G., Gorenstein, P., et al. 1979, ApJ, 234, L51
Healy, K. R., Hester, J. J., & Claussen, M. J. 2004, ApJ, 610, 835
Herbig, G. H., & Dahm, S. E. 2001, PASP, 113, 195
Hester, J. J., Scowen, P. A., Sankrit, R., et al. 1996, AJ, 111, 2349
Hillenbrand, L. A., Massey, P., Strom, S. E., & Merrill, K. M. 1993, AJ, 106, 1906
Hong, J., Schlegel, E. M., & Grindlay, J. E. 2004, ApJ, 614, 508
Indebetouw, R., Robitaille, T. P., Whitney, B. A., et al. 2007, ApJ, 666, 321
Jansen, F., Lumb, D., Altieri, B., et al. 2001, A&A, 365, L1
Linsky, J. L., Gagné, M., Mytyk, A., McCaughrean, M., & Andersen, M. 2007, ApJ, 654, 347
Maggio, A., Flaccomio, E., Favata, F., et al. 2007, ApJ, 660, 1462
Martayan, C., Floquet, M., Hubert, A. M., et al. 2008, A&A, 489, 459
McCaughrean, M. J., & Andersen, M. 2002, A&A, 389, 513
Meaburn, J., & Walsh, J. R. 1986, MNRAS, 220, 745
Montmerle, T., Koch-Miramond, L., Falgarone, E., & Grindlay, J. E. 1983, ApJ, 269, 182
Morrison, R., & McCammon, D. 1983, ApJ, 270, 119
Muzerolle, J., Calvet, N., & Hartmann, L. 2001, ApJ, 550, 944
Nazé, Y., Broos, P. S., Oskinova, L., et al. 2011, ApJS, 194, 7
Owocki, S. P., & Cohen, D. H. 1999, ApJ, 520, 833
Palla, F., & Stahler, S. W. 1993, ApJ, 418, 414
Pallavicini, R., Golub, L., Rosner, R., et al. 1981, ApJ, 248, 279
Pollock, A. M. T., Corcoran, M. F., Stevens, I. R., & Williams, P. M. 2005, ApJ, 629, 482
Preibisch, T., & Feigelson, E. D. 2005, ApJS, 160, 390
Preibisch, T., & Zinnecker, H. 2002, AJ, 123, 1613
Prisinzano, L., Micela, G., Flaccomio, E., et al. 2008, ApJ, 677, 401
Puccetti, S., Fiore, F., D'Elia, V., et al. 2006, A&A, 457, 501
Romanova, M. M., Ustyugova, G. V., Koldoba, A. V., & Lovelace, R. V. E. 2004, ApJ, 616, L151
Sana, H., Gosset, E., & Evans, C. J. 2009, MNRAS, 400, 1479
Siess, L., Dufour, E., & Forestini, M. 2000, A&A, 358, 593
Smith, N. 2006, MNRAS, 367, 763
Smith, R. K., Brickhouse, N. S., Liedahl, D. A., & Raymond, J. C. 2001, ApJ, 556, L91
Stelzer, B., Flaccomio, E., Montmerle, T., et al. 2005, ApJS, 160, 557
Stelzer, B., & Neuhäuser, R. 2001, A&A, 377, 538
Sugitani, K., Watanabe, M., Tamura, M., et al. 2007, PASJ, 59, 507
Townsley, L. K., Broos, P. S., Corcoran, M. F., et al. 2011a, ApJS, 194, 1
Townsley, L. K., Broos, P. S., Corcoran, M. F., et al. 2011b, ApJS, 194, 1
Wang, J., Townsley, L. K., Feigelson, E. D., et al. 2007, ApJS, 168, 100
Wang, J., Townsley, L. K., Feigelson, E. D., et al. 2008, ApJ, 675, 464
Weisskopf, M. C., Brinkman, B., Canizares, C., et al. 2002, PASP, 114, 1
Winston, E., Megeath, S. T., Wolk, S. J., et al. 2010, AJ, 140, 266
Wright, N. J., Drake, J. J., Drew, J. E., & Vink, J. S. 2010, ApJ, 713, 871
Wuchterl, G., & Tscharnuter, W. M. 2003, A&A, 398, 1081
Zhekov, S. A., & Palla, F. 2007, MNRAS, 382, 1124